Editors' Suggestion

Experimental Observation of Tensor Monopoles with a Superconducting Qudit

Xinsheng Tan,[1,*] Dan-Wei Zhang,[2,3,†] Wen Zheng,[1] Xiaopei Yang,[1] Shuqing Song,[1] Zhikun Han,[1] Yuqian Dong,[1] Zhimin Wang,[1] Dong Lan,[1] Hui Yan,[2,3] Shi-Liang Zhu,[2,3,‡] and Yang Yu[1,§]

[1]*National Laboratory of Solid State Microstructures, School of Physics, Nanjing University, Nanjing 210093, China*

[2]*Guangdong Provincial Key Laboratory of Quantum Engineering and Quantum Materials, School of Physics and Telecommunication Engineering, South China Normal University, Guangzhou 510006, China*

[3]*Guangdong-Hong Kong Joint Laboratory of Quantum Matter, Frontier Research Institute for Physics, South China Normal University, Guangzhou 510006, China*

(Received 22 June 2020; accepted 9 December 2020; published 7 January 2021)

Monopoles play a center role in gauge theories and topological matter. There are two fundamental types of monopoles in physics: vector monopoles and tensor monopoles. Examples of vector monopoles include the Dirac monopole in three dimensions and Yang monopole in five dimensions, which have been extensively studied and observed in condensed matter or artificial systems. However, tensor monopoles are less studied, and their observation has not been reported. Here we experimentally construct a tunable spin-1 Hamiltonian to generate a tensor monopole and then measure its unique features with superconducting quantum circuits. The energy structure of a 4D Weyl-like Hamiltonian with threefold degenerate points acting as tensor monopoles is imaged. Through quantum-metric measurements, we report the first experiment that measures the Dixmier-Douady invariant, the topological charge of the tensor monopole. Moreover, we observe topological phase transitions characterized by the topological Dixmier-Douady invariant, rather than the Chern numbers as used for conventional monopoles in odd-dimensional spaces.

DOI: 10.1103/PhysRevLett.126.017702

Introduction.—Monopoles are fundamental topological objects in high-energy physics and condensed matter physics. In 1931, Dirac captured the physical importance of magnetic monopoles (called Dirac monopoles) [1], and proved the quantization of the electric charge. The Dirac monopole was later recognized to be connected to the Berry curvature and Berry phase in quantum mechanics [2]. The topological nature of Dirac monopoles defined in three dimensions is characterized by the first Chern number. Other monopoles have been identified in gauge theory, such as the 't Hooft-Polyakov monopole [3,4] in Yang-Mills theory and the Yang monopole [5]. The Yang monopole is a non-Abelian extension of the Dirac monopole in five dimensions and is characterized by the second Chern number. Generally, a zoo of monopoles in $(2n+1)$-dimensional ($n = 1, 2, 3\ldots$) flat spaces can be identified by the n-order Chern numbers, which are given by the integral of the corresponding field strength associated with a monopole's gauge field [6].

From the aspect of gauge fields, there are two fundamental types of monopoles in physics: vector monopoles associated with vector gauge fields, such as the aforementioned Dirac and Yang monopoles, and tensor monopoles associated with tensor gauge fields [7–10]. A representative of the so-called "tensor monopole" is defined in a four-dimensional (4D) space. The topological charge of a 4D tensor monopole is given by the integral of the tensor gauge field [10–13], known as the Dixmier-Douady (DD) invariant [14,15]. Tensor monopoles play a key role in string theory, where currents naturally couple to a tensor gauge field [16–18]. Recently, Palumbo and Goldman proposed a realistic three-band model defined over a 4D parameter space to generate tensor monopoles [11,12], whose topological charges could be extracted from the generalized Berry curvature by measuring the quantum metric [19–23]. The quantum metric in engineered quantum systems can be measured through periodic driving [24,25], sudden quench [26], and spin texture [27,28].

So far, monopoles have not been observed for real particles. However, they can emerge in condensed-matter materials [29,30] or be engineered in certain artificial systems with effective gauge fields [31–34]. In these systems, monopoles are usually connected to the existence of topological states. For instance, Weyl points in Weyl semimetals can be viewed as fictitious Dirac monopoles in momentum space [30]. The analog Dirac monopoles were created in the synthetic electromagnetic field that arises in the spin texture of atomic spinor condensates [35,36]. The monopole field and the first Chern number were measured in a 3D parameter space of spin-1/2 or spin-1 artificial atoms [37–40]. A quantum-simulated Yang monopole was observed in a 5D parameter space built from an atomic condensate's internal states, and the second Chern number as its topological charge was measured [41]. Although the fundamental importance of singularity points associated with tensor gauge fields was theoretically revealed in

 © 2021 American Physical Society

high-energy physics and condensed matter physics [10–18], the tensor monopoles have not yet been realized or simulated, and the corresponding topological DD invariant has not been measured.

In this Letter, we fill this gap by experimentally synthesizing tensor monopoles in a 4D parameter space built in superconducting quantum circuits and measuring its topological features. By engineering a tunable 4D Weyl-like spin-1 Hamiltonian, we first image the energy structure with threefold degenerate points acting as tensor monopoles. By characterizing the generalized curvature tensor through quantum-metric measurements, we report the first experiment to realize tensor gauge fields and measure the DD invariant as the topological charge of a tensor monopole. Finally, we engineer and observe the topological phase transition characterized by the DD invariant, where the manifold topology changes from a trivial state to a nontrivial one with the modification of a parameter in the Hamiltonian. Our work not only demonstrates the first observation of tensor monopoles and measurement of the DD invariant in a superconducting qudit, but also paves the way to explore high-dimensional topological defects in fully engineered quantum systems. The experimental observation of tensor monopoles can further our understanding of tensor gauge fields and advance the search for new exotic topological matter in condensed matter physics and artificial quantum systems.

Tensor monopoles and tensor fields.—To establish a basic understanding of the tensor monopole in 4D parameter space, we begin by comparing it with the well-known Dirac monopole in three dimensions, both spanned by the parameters $\boldsymbol{q}$, as shown in Fig. 1. For a nondegenerate quantum state $|u_{\boldsymbol{q}}\rangle$, the geometric property is captured by a quantum geometric tensor [19,42,43]: $\chi_{\mu\nu} = \langle \partial_{q_\mu} u_{\boldsymbol{q}} | (1 - |u_{\boldsymbol{q}}\rangle\langle u_{\boldsymbol{q}}|) | \partial_{q_\nu} u_{\boldsymbol{q}} \rangle = g_{\mu\nu} + i\mathcal{F}_{\mu\nu}/2$, where the real and imaginary parts define the quantum metric $g_{\mu\nu} = g_{\nu\mu}$ and Berry curvature (gauge field) $\mathcal{F}_{\mu\nu} = -\mathcal{F}_{\nu\mu}$, respectively. The Berry curvature $\mathcal{F}_{\mu\nu} = \partial_\mu A_\nu - \partial_\nu A_\mu$ with the Berry connection $A_\mu = i\langle u_{\boldsymbol{q}} | \partial_{q_\mu} u_{\boldsymbol{q}} \rangle$ is associated with the Berry phase. The quantum metric $g_{\mu\nu}$ defines the quantum distance between nearby states $|u_{\boldsymbol{q}}\rangle$ and $|u_{\boldsymbol{q}+d\boldsymbol{q}}\rangle$ in the parameter space [19–23]: $ds^2 = 1 - |\langle u_{\boldsymbol{q}} | u_{\boldsymbol{q}+\delta\boldsymbol{q}} \rangle|^2 = \sum_{\mu\nu} g_{\mu\nu} dq_\mu dq_\nu$, which is related to the wave function overlap and can thus be directly measured.

For a Dirac monopole in 3D $\boldsymbol{q}$ space, in the context of gauge field (electromagnetism), the Berry curvature $\mathcal{F}_{\mu\nu}$ can be viewed as the field strength (the Faraday tensor) associated with the flux through the surrounding sphere S^2 with radius $r = |\boldsymbol{q}|$. A minimal model realizing a Dirac monopole is the Weyl Hamiltonian $H_{3D} = \boldsymbol{q} \cdot \boldsymbol{\sigma}$, where $\boldsymbol{\sigma} = (\sigma_x, \sigma_y, \sigma_z)$ are the Pauli matrices. The topological charge of the Dirac monopole at $\boldsymbol{q} = 0$ is then given by the first Chern number $C_1 = (1/2\pi) \int_{S^2} \mathcal{F} = 1$. Notably, the Berry curvature associated with a monopole is related to the determinant of the metric tensor $g_{\mu\nu}$ defined on a sphere with $\mu, \nu = \{\theta, \phi\}$: $\mathcal{F}_{\mu\nu} = 2\epsilon_{\mu\nu}\sqrt{\det(g_{\mu\nu})}$, where $\epsilon_{\mu\nu}$ is the Levi-Civita symbol, $g_{\theta\theta} = 1/4$, $g_{\phi\phi} = \sin^2\theta/4$, and $g_{\theta\phi} = 0$.

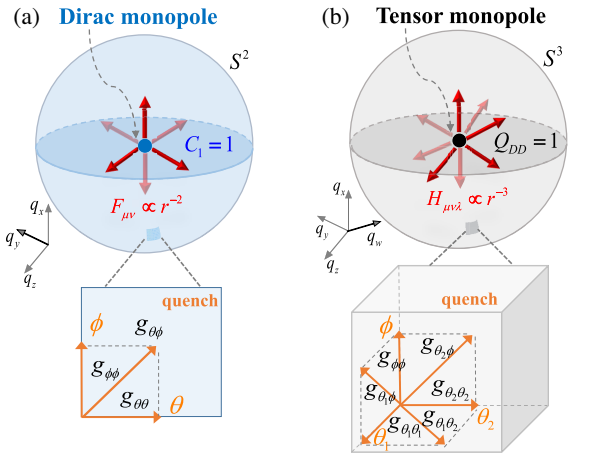

FIG. 1. Pictorial representations of (a) a Dirac monopole in 3D parameter space $\boldsymbol{q} = (q_x, q_y, q_z)$; and (b) a tensor monopole in 4D parameter space $\boldsymbol{q} = (q_x, q_y, q_z, q_w)$. The two are defined as pointlike sources of vector and tensor gauge fields, respectively. The fluxes associated with the field strengths $\mathcal{F}_{\mu\nu} \propto r^{-2}$ and $\mathcal{H}_{\mu\nu\lambda} \propto r^{-3}$ through the surrounding 2D and 3D spheres (S^2 and S^3) with radius $r = |\boldsymbol{q}|$ are quantized in terms of two different topological invariants, the first Chern number $C_1 = 1$ and the DD invariant $Q_{\mathrm{DD}} = 1$, respectively. The related quantum metric tensors $g_{\mu\nu}$ in S^2 and S^3 can be measured from the quench scheme.

Different from the odd-dimensional monopoles defined with vector fields, a tensor monopole is defined in even dimensions and associated with tensor fields. A tensor monopole in 4D space $\boldsymbol{q} = (q_x, q_y, q_z, q_z)$ takes a (3-form) curvature tensor $\mathcal{H}_{\mu\nu\lambda}$ [11,12], as the generalization of the (2-form) Berry curvature $\mathcal{F}_{\mu\nu}$ of the Dirac monopole. A minimal model realizing such a tensor monopole is the three-band Weyl-like Hamiltonian in 4D space [11]:

$$H_{4D} = \boldsymbol{q} \cdot \boldsymbol{\lambda} = \begin{bmatrix} 0 & q_x - iq_y & 0 \\ q_x + iq_y & 0 & q_z + iq_w \\ 0 & q_z - iq_w & 0 \end{bmatrix}, \qquad (1)$$

where $\lambda = (\lambda_1, \lambda_2, \lambda_6, \lambda_7^*)$ are 3×3 Gell-Mann matrices. The energy spectrum is given by $E_{0,\pm} = 0, \pm|\boldsymbol{q}|$, with a triple-degenerate Weyl-like point at $\boldsymbol{q} = (0, 0, 0, 0)$ in 4D parameter space. Such a Weyl-like node gives a tensor monopole, surrounded by a 3D hypersphere S^3. In terms of hyperspherical coordinates $\{r, \theta_1, \theta_2, \phi\}$ ($\theta_{1,2} \in [0, \pi]$ and $\phi \in [0, 2\pi]$), one has $q_x = r\cos\theta_1$, $q_y = r\sin\theta_1\cos\theta_2$, $q_z = r\sin\theta_1\sin\theta_2\cos\phi$, and $q_w = r\sin\theta_1\sin\theta_2\sin\phi$. The generalized curvature tensor as the field strength in S^3 is related to the quantum metric [11]:

$$\mathcal{H}_{\theta_1\theta_2\phi} = \epsilon_{\theta_1\theta_2\phi}(4\sqrt{\det g_{\mu\nu}}), \qquad \mu,\nu = \{\theta_1,\theta_2,\phi\}. \quad (2)$$

Here H_{4D} has ϕ-rotation symmetry and thus $\mathcal{H}_{\theta_1\theta_2\phi}$ is independent of ϕ. For the ground state $|\psi_-\rangle$ of the system, all matrix elements of the metric tensor g can be explicitly obtained [see Eqs. (S7) in the Supplemental Material [44]]. The tensor monopole generalizes the Dirac monopole to four dimensions, and takes a topological charge associated with the generalized curvature tensor $\mathcal{H}_{\theta_1\theta_2\phi}$:

$$Q_{\mathrm{DD}} = \frac{1}{2\pi^2}\int_0^{\pi} d\theta_1 \int_0^{\pi} d\theta_2 \int_0^{2\pi} d\phi \mathcal{H}_{\theta_1\theta_2\phi} = 1, \quad (3)$$

which is the DD invariant [14,15]. Thus, to obtain the topological charge Q_{DD} of a tensor monopole, one can measure $\mathcal{H}_{\theta_1\theta_2\phi}$ by revealing the quantum metric $g_{\mu\nu}$.

In parameter space, the quantum distance ds^2 is related to the transition probability P^+ of the quantum state being excited to other eigenstates after a sudden quench: $P^+ = ds^2$ [19,20,26]. One can thus measure the quantum metric via transition probability by the sudden quench method. For a quantum state initially prepared at $\boldsymbol{q}$, to extract the diagonal components $g_{\mu\mu}$ at this point, one can suddenly quench the system parameter to $\boldsymbol{q} + \delta q \boldsymbol{e}_\mu$ along the $\boldsymbol{e}_\mu$ direction, and then measure the transition probability $P^+_{\mu\mu} = g_{\mu\mu}\delta q^2 + \mathcal{O}(\delta q^3)$. To extract the off-diagonal components $g_{\mu\nu}$ $(\mu \neq \nu)$, we apply a sudden quench to $\boldsymbol{q} + \delta q \boldsymbol{e}_\mu + \delta q \boldsymbol{e}_\nu$ along the $\boldsymbol{e}_\mu + \boldsymbol{e}_\nu$ direction and then measure the probability $P^+_{\mu\nu}$, which has the relation $P^+_{\mu\nu} - P^+_{\mu\mu} - P^+_{\nu\nu} = 2g_{\mu\nu}\delta q^2 + \mathcal{O}(\delta q^3)$. This sudden quench scheme will be used to measure the quantum metric $g_{\mu\nu}$ in Eq. (2).

Experimental system.—We realize a highly tunable spin-1 Hamiltonian with superconducting quantum circuits and observe the energy spectrum and topological charge of the tensor monopole in parameter space. The circuits consist of a superconducting transmon qubit embedded in a 3D aluminum cavity [39,40,48–51]. The resonance frequency of the cavity TE101 mode is 9.0526 GHz. The whole sample package is cooled in a dilution refrigerator to a base temperature of 20 mK. The experimental setup for the qubit control and measurement is well established [39,40,48–51]. The coupled transmon qubit and cavity exhibit anharmonic multiple energy levels. In our experiments, the lowest four energy levels $|0\rangle$, $|1\rangle$, $|2\rangle$, and $|3\rangle$ are used and form a qudit system shown in Fig. 2(a). Among them, three levels are chosen to construct the Hamiltonian in Eq. (4), which are $\{1,2,3\}$ and $\{0,1,2\}$ for measurements of energy structures and quantum metric, respectively [44]. Microwave fields are applied to couple the four energy levels. The transition frequencies between them are $\omega_{10}/2\pi = 7.1194$, $\omega_{12}/2\pi = 6.7747$, and $\omega_{23}/2\pi = 6.3926$ GHz, respectively, which are independently determined by saturation spectroscopy [44]. We apply microwave driving along x, y, and z directions and realize the following effective Hamiltonian in the rotating frame ($\hbar = 1$) [44]

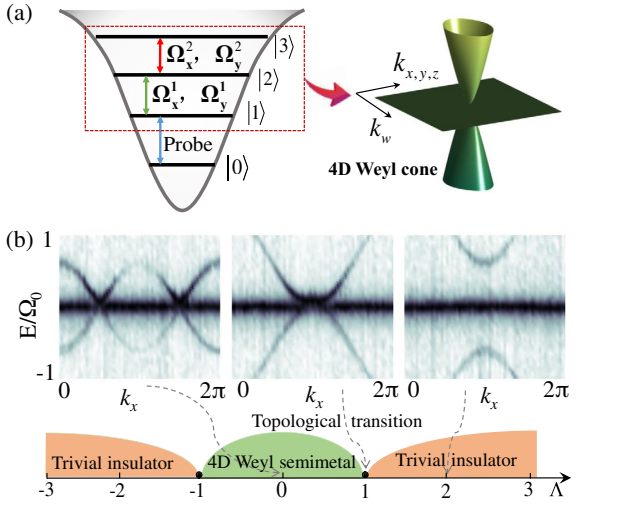

FIG. 2. Measurement of the energy structure of a 4D Weyl-like semimetal. (a) Diagram of energy levels in superconducting circuit. $|1\rangle$, $|2\rangle$, and $|3\rangle$ are used to construct the Hamiltonian with irradiated microwaves, while $|0\rangle$ is for detecting the spectrum. (b) Measured energy structure with different offsets $\Lambda = 0, 1, 2$ in the phase diagram.

$$H_{\mathrm{exp}} = \frac{1}{2}\begin{bmatrix} 0 & \Omega_x^1 - i\Omega_y^1 & 0 \\ \Omega_x^1 + i\Omega_y^1 & 0 & \Omega_x^2 + i\Omega_y^2 \\ 0 & \Omega_x^2 - i\Omega_y^2 & 0 \end{bmatrix}, \quad (4)$$

where $\Omega_x^{1(2)}$ $(\Omega_y^{1(2)})$ is the Rabi frequency along the x (y) axis of the Bloch sphere spanned by the corresponding basis. For the case shown in Fig. 2(a), the system parameters $\Omega_{x,y}^1$ $[(\Omega_{x,y}^2)]$ are fully controlled by the amplitude and phase of the microwave applied to couple $|1\rangle$ and $|2\rangle$ ($|2\rangle$ and $|3\rangle$). By varying these parameters, we can create arbitrary three-level Hamiltonians given by Eq. (4). In our experiments, we work with collections of Hamiltonians represented in the 4D parameter space by accurately designing microwave fields after calibration of the parameters using Rabi oscillations and Ramsey fringes [44].

Measuring energy structures of 4D Weyl model.—We obtain the energy structure by measuring the spectrum of the qudit system. After mapping the momentum space of a 4D Weyl-semimetal Hamiltonian [12,44] to the parameter space of the system Hamiltonian in Eq. (4), we can visualize the simulated energy structures. We design the Rabi frequencies $\{\Omega_x^1,\Omega_y^1,\Omega_x^2,\Omega_y^2\} = \{\Omega_0(3+\Lambda-\cos k_x-\cos k_y-\cos k_z-\cos k_w, \Omega_0 \sin k_y, \Omega_0 \sin k_z, \Omega_0 \sin k_w\}$, where $\Omega_0 = 5$ MHz is the energy unit and the parameter Λ is added to account for an offset in Ω_x^1. As shown in Fig. 2(a), the energy levels $\{|1\rangle, |2\rangle, |3\rangle\}$ are used to construct H_{exp} and $|0\rangle$ is treated as a reference level for spectrum probing. The dressed states under the coupled microwaves are eigenstates of the Hamiltonian (4) labeled $|\psi_0\rangle$ and $|\psi_\pm\rangle$. Notably, the fictitious momenta

$k_{x,y,z,w}$ (the indexes x, y, z are not related to real spatial coordinates of the experimental system) denote the 4D parameter space controlled by varying $\Omega_{x,y}^{1,2}$ in our system and Λ plays the role of a fictitious Zeeman field for tuning topological phase transition [12,44]. Similar mapping procedures were used to simulate other condensed-matter models in engineered quantum systems [37–41].

In our routine, we execute the spectrumlike measurement and the resonant peaks of microwave absorption are detected [44]. The frequency of the resonant peak is a function of $k_{x,y,z,w}$, and we are able to extract the energy structure of the 4D Weyl-like cone, as illustrated in the right panel of Fig. 2(a). To demonstrate the topological properties, we set $k_{y,z,w} = 0$ to emphasize the E-k_x plane, where the phase transition can be clearly observed. The system has two different phases determined by the parameter Λ, as shown in Fig. 2(b): the 4D Weyl-like semimetal with a pair of 4D Weyl points when $|\Lambda| < 1$ and the trivial gapped insulator when $|\Lambda| > 1$ [11,12]. At the critical points $|\Lambda| = 1$, two degenerate points merge and then disappear. The extracted energy structures for $\Lambda = 0$, 1, 2 are illustrated in Fig. 2(b), which capture the features of the theoretical prediction with two degenerate points at $K_{\pm} = (\pm\pi/2, 0, 0, 0)$ when $\Lambda = 0$. Near $K_{\pm}$, one has the low-energy effective Hamiltonian $H_{4D}^{\pm} = \pm q_x\lambda_1 + q_y\lambda_2 + q_z\lambda_6 + q_w\lambda_7^*$ describing a pair of tensor monopoles with $Q_{DD} = \pm 1$ [44], where the sign in front of q_x determines the topological charges. Below we focus on the tensor monopole described by $H_{4D}^{+} = H_{4D}$ in Eq. (1) and $Q_{DD} = 1$.

Measuring quantum metric by sudden quench.—We now measure the quantum metric $g_{\mu\nu}$ ($\mu, \nu = \{\theta_1, \theta_2, \phi\}$) of the simulated tensor monopole using the sudden quench scheme. We here work with the three lowest-energy levels $\{|0\rangle, |1\rangle, |2\rangle\}$ without a reference level since the spectrum probing is unnecessary [44]. We construct the Hamiltonian in hypersphere coordinates with parameters in Eq. (4) as $\{\Omega_x^1 = \Omega_0 \cos\theta_1, \Omega_y^1 = \Omega_0 \sin\theta_1 \cos\theta_2, \Omega_x^2 = \Omega_0 \sin\theta_1 \sin\theta_2 \cos\phi, \Omega_y^2 = \Omega_0 \sin\theta_1 \sin\theta_2 \sin\phi\}$ [44]. The system is initially prepared in the ground state $|\psi_-\rangle$ in the parameter space $\boldsymbol{q} = \{\theta_1, \theta_2, \phi\}$ with $\phi = 0$. The Hamiltonian is then rapidly swept to $H(\boldsymbol{q} + \delta\boldsymbol{q})$, followed by state tomography to obtain the transition probability. We set the quench parameter to $\boldsymbol{q}(t) = \boldsymbol{q} + t/T\delta q\boldsymbol{e}$ along the $\boldsymbol{e}$ direction, where the quench time $T = 9$ ns and $\delta q = \pi/8$ or $\pi/16$ [44]. For the diagonal term $g_{\mu\mu}$, only one parameter ramps linearly in each quench with $\boldsymbol{e} = \{\boldsymbol{e}_{\theta_1}, \boldsymbol{e}_{\theta_2}, \boldsymbol{e}_{\phi}\}$, respectively. For the off-diagonal term $g_{\mu\nu}$ ($\mu \neq \nu$), the parameters μ and ν ramp simultaneously, with $\boldsymbol{e} = \{\boldsymbol{e}_{\theta_1} + \boldsymbol{e}_{\theta_2}, \boldsymbol{e}_{\theta_1} + \boldsymbol{e}_{\phi}, \boldsymbol{e}_{\theta_2} + \boldsymbol{e}_{\phi}\}$. These ramp procedures are illustrated in Fig. 1(b). From the final state's tomography, we extract the metric at $\boldsymbol{q}$ from the measured transition probability: $g_{\mu\mu} \approx P_{\mu\mu}/\delta q^2$ and $g_{\mu\nu} \approx (P_{\mu\nu} - P_{\mu\mu} - P_{\nu\nu})/2\delta q^2$. The measured $g_{\mu\nu}$ as a function of θ_1 and θ_2 are shown in Fig. 3, which agree well with theoretical results.

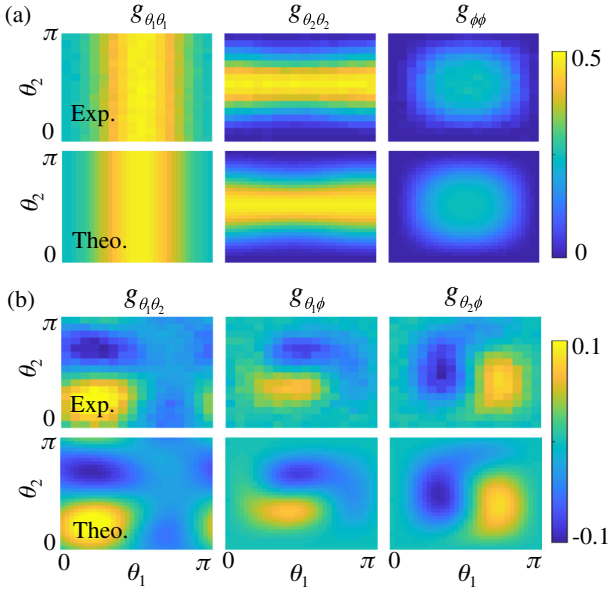

FIG. 3. Experimental and theoretical results of the quantum metric $g_{\mu\nu}$ as a function of θ_1 and θ_2 for (a) diagonal components; and (b) off-diagonal components.

Observing topological phase transitions.—To further study the tensor monopole, we observe topological phase transition characterized by the tensor monopole charge in our superconducting circuits. By designing microwave fields on the qudit, we modify Eq. (4) by adding a tunable offset Λ into the Ω_x^1 term, such that $\Omega_x^1 = \Omega_0(\cos\theta_1 + \Lambda)$, while other terms remain unchanged (without breaking the ϕ-rotation symmetry). By measuring the metric tensor with the sudden-quench approach, we can obtain the generalized curvature $\mathcal{H}_{\theta_1\theta_2\phi}$ and then integrate it to derive the topological charge Q_{DD}. For offset $\Lambda = 0$, the extracted $\mathcal{H}_{\theta_1\theta_2\phi}$ as a function of parameters θ_1 and θ_2 is shown in Fig. 4(a). Experimental data (left) agree with theoretical results (right). We finally calculate the Q_{DD} using Eq. (3) and obtain $Q_{DD} = 0.92 \pm 0.15$ for $\Lambda = 0$.

To study the topological phase transition, we execute the protocol with varying Λ. The extracted DD invariant as a function of Λ is shown in Fig. 4(b). When $|\Lambda| = 0$, the manifold of the parameter space S^3 surrounds the tensor monopole in the center. With the increase of $|\Lambda|$, the tensor monopole moves along the q_x axis. $Q_{DD} \approx 1$ when $|\Lambda| < 1$ for the S^3 sphere surrounding the tensor monopole. $Q_{DD} \approx 0$ when $|\Lambda| > 1$ since the monopole moves outside the hypersphere manifold, indicating that the system is in the trivial insulator phase. Q_{DD} declines rapidly to around 0 in the vicinity of $\Lambda = \pm 1$, which indicates a topological phase transition. The accuracy of the topological charge extracting from the sudden quench routine depends on the ramp step. In Fig. 4(b), the numerical results with $\delta q = \pi/1024$ are plotted, which are very close to the expected integer values. However, such a small step is not feasible to implement in practice due to limitation of

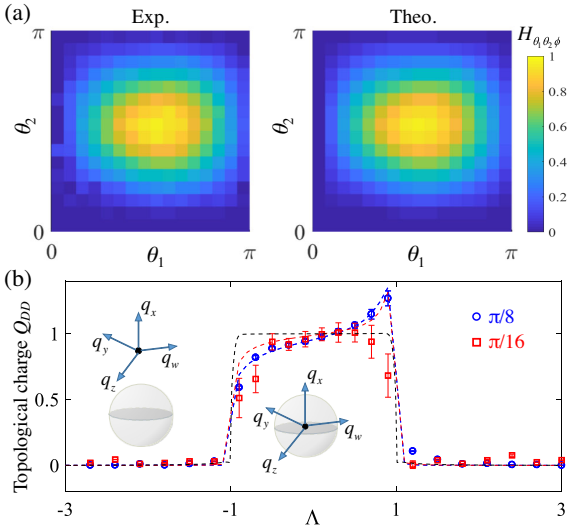

FIG. 4. Topological phase transition characterized by tensor monopole charge. (a) Experimental and theoretical results of generalized curvature tensor $\mathcal{H}_{\theta_1\theta_2\phi}$ as a function of θ_1 and θ_2. (b) Topological charge Q_{DD} as a function of offset Λ. $Q_{\mathrm{DD}} \approx 1$ declines rapidly to $Q_{\mathrm{DD}} \approx 0$ when $|\Lambda| > 1$ with the tensor monopole outside the S^3 sphere, indicating topological transition. Data obtained with $\delta q = \pi/8$, and $\pi/16$ are shown in blue and red, respectively, with symbols and dashed lines representing experimental data and numerical simulations, respectively. The black dashed line is the simulation result for $\delta q = \pi/1024$. Some deviations between the experimental and simulation results for $\delta q = \pi/16$ are due to the reduction of the measurement accuracy of the excitation probability in our quench scheme for smaller δq.

readout fidelity. With a larger δq, measurement obtained from the sudden quench routine will deviate from ideal values. For comparison, we perform the routine with $\delta q = \pi/8$ and $\pi/16$, as demonstrated in Fig. 4(b). When δq decreases, the deviation from the ideal quantized values becomes smaller.

Conclusion.—In summary, we have created tensor monopoles in 4D parameter space and explored their unique properties using superconducting circuits. Our experimental observation contributes to exploring tensor gauge fields in quantum mechanics and creates a unique approach in the search for exotic topological matter in condensed matter physics and artificial systems, such as topological semimetals and unconventional quasiparticles beyond Dirac and Weyl fermions in high dimensions. By coupling individual superconducting qudits, one can further explore the geometric and topological properties of quantum many-body systems.

This work was supported by the National Key Research and Development Program of China (Grant No. 2016YFA0301800), the National Natural Science Foundation of China (Grants No. 11474153, No. 91636218, No. 11890704, No. 61521001, No. 12074180, No. U1830111, No. 12074179, No. U1801661, and No. 11822403), the Key-Area Research and Development Program of Guangdong Province (Grants No. 2018B030326001 and No. 2019B030330001), and the Key Project of Science and Technology of Guangzhou (Grants No. 201804020055 and No. 2019050001).

X. T. and D.-W. Z contributed equally to this work.

Note added.—Recently, we noticed another work on experimental observation of the tensor monopole using a single nitrogen-vacancy center in diamond [52].

*tanxs@nju.edu.cn
†danweizhang@m.scnu.edu.cn
‡slzhu@nju.edu.cn
§yuyang@nju.edu.cn

[1] P. A. M. Dirac, Proc. R. Soc. A **133**, 60 (1931).
[2] D. Xiao, M.-C. Chang, and Q. Niu, Rev. Mod. Phys. **82**, 1959 (2010).
[3] A. M. Polyakov, JETP Lett. **20**, 194 (1974).
[4] G. 't Hooft, Nucl. Phys. **B79**, 276 (1974).
[5] C. N. Yang, Math. Phys. Appl. Math. **19**, 320 (1978).
[6] M. Nakahara, *Geometry, Topology, and Physics* (Institute of Physics Publishing, Bristol, 2003).
[7] R. I. Nepomechie, Phys. Rev. D **31**, 1921 (1985).
[8] C. Teitelboim, Phys. Lett. **167B**, 69 (1986).
[9] P. Orland, Nucl. Phys. **B205**, 107 (1982).
[10] M. Kalb and P. Ramond, Phys. Rev. D **9**, 2273 (1974).
[11] G. Palumbo and N. Goldman, Phys. Rev. Lett. **121**, 170401 (2018).
[12] G. Palumbo and N. Goldman, Phys. Rev. B **99**, 045154 (2019).
[13] Y.-Q. Zhu, N. Goldman, and G. Palumbo, Phys. Rev. B **102**, 081109(R) (2020).
[14] V. Mathai and G. C. Thiang, Commun. Math. Phys. **355**, 561 (2017).
[15] M. K. Murray, J. Lond. Math. Soc. **54**, 403 (1996).
[16] T. Banks and N. Seiberg, Phys. Rev. D **83**, 084019 (2011).
[17] N. E. Mavromatos and S. Sarkar, Phys. Rev. D **95**, 104025 (2017).
[18] M. Montero, A. M. Uranga, and I. Valenzuela, J. High Energy Phys. 07 (2017) 123.
[19] M. Kolodrubetz, D. Sels, P. Mehta, and A. Polkovnikov, Phys. Rep. **697**, 1 (2017).
[20] L.-K. Lim, J.-N. Fuchs, and G. Montambaux, Phys. Rev. A **92**, 063627 (2015).
[21] J. P. Provost and G. Vallee, Commun. Math. Phys. **76**, 289 (1980).
[22] Y.-Q. Ma, S. Chen, H. Fan, and W.-M. Liu, Phys. Rev. B **81**, 245129 (2010).
[23] A. T. Rezakhani, D. F. Abasto, D. A. Lidar, and P. Zanardi, Phys. Rev. A **82**, 012321 (2010).
[24] T. Ozawa and N. Goldman, Phys. Rev. B **97**, 201117(R) (2018).

[25] M. Yu, P. Yang, M. Gong, Q. Cao, Q. Lu, H. Liu, M. B. Plenio, F. Jelezko, T. Ozawa, N. Goldman, S. Zhang, and J. Cai, Natl. Sci. Rev. **7**, 254 (2020).
[26] X. Tan, D.-W. Zhang, Z. Yang, J. Chu, Y.-Q. Zhu, D. Li, X. Yang, S. Song, Z. Han, Z. Li, Y. Dong, H.-F. Yu, H. Yan, S.-L. Zhu, and Y. Yu, Phys. Rev. Lett. **122**, 210401 (2019).
[27] O. Bleu, D. D. Solnyshkov, and G. Malpuech, Phys. Rev. B **97**, 195422 (2018).
[28] A. Gianfrate, O. Bleu, L. Dominici, V. Ardizzone, M. De Giorgi, D. Ballarini, G. Lerario, K. W. West, L. N. Pfeiffer, D. D. Solnyshkov, D. Sanvitto, and G. Malpuech, Nature (London) **578**, 381 (2020).
[29] X. L. Qi and S. C. Zhang, Rev. Mod. Phys. **83**, 1057 (2011).
[30] N. P. Armitage, E. J. Mele, and A. Vishwanath, Rev. Mod. Phys. **90**, 015001 (2018).
[31] J. Dalibard, F. Gerbier, G. Juzeliunas, and P. Ohberg, Rev. Mod. Phys. **83**, 1523 (2011).
[32] N. Goldman, G. Juzeliunas, P. Ohberg, and I. B. Spielman, Rep. Prog. Phys. **77**, 126401 (2014).
[33] D.-W. Zhang, Y.-Q. Zhu, Y. X. Zhao, H. Yan, and S.-L. Zhu, Adv. Phys. **67**, 253 (2018).
[34] T. Ozawa, H. M. Price, A. Amo, N. Goldman, M. Hafezi, L. Lu, M. C. Rechtsman, D. Schuster, J. Simon, O. Zilberberg, and I. Carusotto, Rev. Mod. Phys. **91**, 015006 (2019).
[35] M. W. Ray, E. Ruokokoski, S. Kandel, M. Mottonen, and D. S. Hall, Nature (London) **505**, 657 (2014).
[36] M. W. Ray, E. Ruokokoski, K. Tiurev, M. Mottonen, and D. S. Hall, Science **348**, 544 (2015).
[37] M. D. Schroer, M. H. Kolodrubetz, W. F. Kindel, M. Sandberg, J. Gao, M. R. Vissers, D. P. Pappas, A. Polkovnikov, and K. W. Lehnert, Phys. Rev. Lett. **113**, 050402 (2014).
[38] P. Roushan, C. Neill, Y. Chen, M. Kolodrubetz, C. Quintana, N. Leung, M. Fang, R. Barends, B. Campbell, Z. Chen *et al.*, Nature (London) **515**, 241 (2014).
[39] X. Tan, D.-W. Zhang, Q. Liu, G. Xue, H.-F. Yu, Y.-Q. Zhu, H. Yan, S.-L. Zhu, and Y. Yu, Phys. Rev. Lett. **120**, 130503 (2018).
[40] X. Tan, Y. X. Zhao, Q. Liu, G. M. Xue, H.-F. Yu, Z. D. Wang, and Y. Yu, Phys. Rev. Lett. **122**, 010501 (2019).
[41] S. Sugawa, F. Salces-Carcoba, A. R. Perry, Y. Yue, and I. B. Spielman, Science **360**, 1429 (2018).
[42] A. Carollo, D. Valenti, and B. Spagnolo, Phys. Rep. **838**, 1 (2020).
[43] S. L. Zhu, Int. J. Mod. Phys. B **22**, 561 (2008).
[44] See Supplemental Material at http://link.aps.org/supplemental/10.1103/PhysRevLett.126.017702 for more details, which includes Refs. [45–47], which are not already in the Letter.
[45] M. D. Reed, L. DiCarlo, B. R. Johnson, L. Sun, D. I. Schuster, L. Frunzio, and R. J. Schoelkopf, Phys. Rev. Lett. **105**, 173601 (2010).
[46] H. Chen, M. Hu, J.Chen, and J. Du, Phys. Rev. A **80**, 054101 (2009).
[47] S. Berger, M. Pechal, S. Pugnetti, A. A. Abdumalikov, L. Steffen, A. Fedorov, A. Wallraff, and S. Filipp, Phys. Rev. B **85**, 220502(R) (2012).
[48] H. Paik, D. I. Schuster, L. S. Bishop, G. Kirchmair, G. Catelani, A. P. Sears, B. R. Johnson, M. J. Reagor, L. Frunzio, L. I. Glazman, S. M. Girvin, M. H. Devoret, and R. J. Schoelkopf, Phys. Rev. Lett. **107**, 240501 (2011).
[49] D. Riste, J. G. van Leeuwen, H. S. Ku, K. W. Lehnert, and L. DiCarlo, Phys. Rev. Lett. **109**, 050507 (2012).
[50] P. Campagne-Ibarcq, E. Flurin, N. Roch, D. Darson, P. Morfin, M. Mirrahimi, M. H. Devoret, F. Mallet, and B. Huard, Phys. Rev. X **3**, 021008 (2013).
[51] X. Y. Jin, A. Kamal, A. P. Sears, T. Gudmundsen, D. Hover, J. Miloshi, R. Slattery, F. Yan, J. Yoder, T. P. Orlando, S. Gustavsson, and W. D. Oliver, Phys. Rev. Lett. **114**, 240501 (2015).
[52] M. Chen, C. Li, G. Palumbo, Y.-Q. Zhu, N. Goldman, and P. Cappellaro, arXiv:2008.00596.